AN-92-4-3

5646

THE INFLUENCE OF SUPPLY AND EXHAUST OPENINGS ON VENTILATION EFFICIENCY IN AN AIR-CONDITIONED ROOM WITH A RAISED FLOOR

S. Murakami, D.Eng.
Member ASHRAE

S. Kato, D.Eng.
Member ASHRAE

T. Tanaka, D.Eng.

D.-H. Choi

T. Kitazawa

ABSTRACT

A raised-floor air-conditioning system is an effective method for dealing with unevenly distributed heat loads in a room because in this system supply openings can be precisely allocated in relation to the locations of the heat loads. This advantage can be further enhanced by proper design of exhaust openings from the viewpoint of ventilation efficiency.

Experiments and numerical simulations of flow and temperature fields in a room with raised-floor air conditioning analyze its ventilation efficiency. The room used is a model computer room with raised-floor air conditioning.

The purpose of this study is to determine the most effective method for exhausting the large amount of heat generated by such various electric machines as computers in a room with a raised-floor air-conditioning system. Supply openings in the raised floor and exhausts in the ceiling are so installed that the supply and exhaust airflow rates are balanced locally in the small space allotted to each supply opening. This ventilation system is intended to prevent formation of a large recirculating flow through the whole room that would convect and mix any heat generated in the room throughout the whole space, resulting in low ventilation efficiency.

Experiments and numerical simulations are performed for the following five cases: (1) supply and exhaust airflow rates are locally balanced, with no heat generation by the computer model; (2) the same local balance as in case 1 but with heat generation by the computer; (3) airflow rates allotted to the exhaust openings just above the computer are greater than those of the other exhaust openings; (4) airflow rates allotted to the exhaust openings just above the computer are less than those of the other exhaust openings; and (5) supply and exhaust airflow rates are not locally balanced, and a large recirculating airflow is thereby formed in the room.

The above-mentioned experiments and numerical simulations support the following conclusions:

1. *Numerical simulations reproduce the observed flow and temperature fields with sufficient accuracy.*
2. *In raised-floor air-conditioned rooms, local air balance of the exhaust and supply airflows yields sufficiently high ventilation efficiency.*

INTRODUCTION

The cooling loads of office air conditioners have increased significantly recently because of an increase in various types of heat sources such as electric machinery. In particular, the increased numbers of personal computers, engineering workstations, mainframes, etc., which generate a large amount of heat, cause serious air-conditioning problems. How to exhaust such heat loads effectively and how to air-condition rooms efficiently have become major concerns for air-conditioning engineers.

The raised-floor system in offices is useful not only for its underfloor electric cabling but also for its cooling and personal air-conditioning system (Arnold 1990; Spoormaker 1990; Heinemeier et al. 1990; Sodec and Craig 1990; Hanzawa and Nagasawa 1990). In the system, cooled air is supplied into the room from the space between the raised floor and the original slab floor. The primary concern of air-conditioning engineers has been control of the air distribution by means of supply jets discharged from openings in the raised floor. That is, engineers up to the present have been generally concerned with the system for supplying conditioned air into the room. However, we believe that the raised-floor system has the potential to become even more efficient when combined with a properly designed exhaust system.

Shuzo Murakami is a professor and **Shinsuke Kato** is an associate professor at the Institute of Industrial Science, University of Tokyo, Japan. **Toshihiko Tanaka** is a researcher at the Institute of Industrial Science and at the Engineering Research Center, Tokyo Electric Power Company. **Dong-Ho Choi** is a post-graduate student at the University of Tokyo. **Tomokazu Kitazawa** is a contract researcher at the Institute of Industrial Science and a researcher at the Toyoko Global Environment Institute Co. Ltd., Kanagawa, Japan.

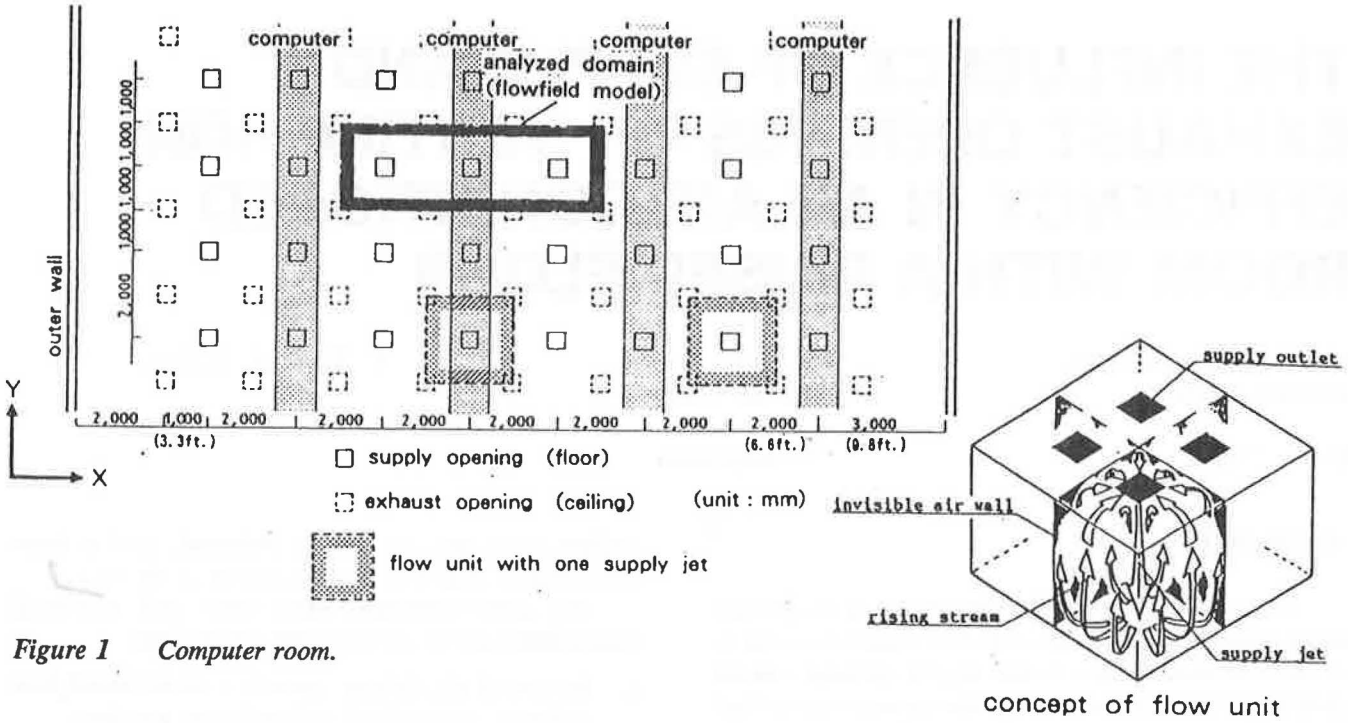

Figure 1 Computer room.

Flow Unit and Locally Balanced Air Supply and Exhaust Ventilation

The concept of the local "flow unit" was introduced by several of the present authors when researching room air distribution of conventional-flow-type clean rooms (Murakami et al. 1987, 1988, 1989, 1990a). We emphasized that the flow and diffusion fields of a conventional-flow-type clean room can be modeled as the serial combination of local flow units, each of which consists of a supply jet and the reverse flows around it. (The concept of the local flow unit is illustrated in Figure 1.) We also noted that contaminant discharged into one local flow unit would not diffuse widely within the room when the air-exhaust opening is installed in the same flow unit and the air-exhaust rate is identical with or more than the air-supply rate of the flow unit. (Murakami et al. 1990b).

These room airflow characteristics can be used to control the purity and temperature of room air. The ventilation system, in particular the one with a locally balanced supply and exhaust airflow rate in each flow unit, also seems useful for the raised-floor air-conditioning system with respect to the rapid exhaust of the heat discharged by electric machinery, although the buoyancy effect of the heated air would have some influence on the flow fields. This study aims to confirm the effectiveness of locally balanced supply-exhaust airflow rate ventilation in the case of nonisothermal airflow with a raised-floor air-conditioning system as well as in the previously studied case in which it was applied to the isothermal conventional-flow-type clean room (Murakami et al. 1988, 1990b). The influence of computer-discharged heat on flow and temperature distributions is also analyzed in detail.

Analyses with Simulations and Experiments

Experiments and numerical simulations were conducted using a flow-field model that is one section of a full computer room with a raised-floor air-conditioning system. The air exhaust system is installed in the ceiling, whereas the air-supply system is in the raised floor of this model. The exhaust inlets are arranged in zigzag fashion with respect to the positions of the supply outlets. That is, the exhaust inlets and supply outlets alternate with each other.

Model experiments were conducted using a one-third scale model. Numerical simulations of turbulent nonisothermal flow were conducted by means of the k-ε model (Viollet 1987; Murakami et al. 1991). The results of the simulations are compared with those of the experiments. The validity of the numerical analyses in this study is confirmed here by the good correspondence between the simulations and the experiments, which thereby allows detailed analyses of flow and temperature fields by means of the simulation technique.

MODEL ROOM ANALYZED

Figure 1 shows the plan of the computer room analyzed. The mainframes of the computer are installed throughout the floor. Air supply openings are in the raised floor, and exhaust openings are in the ceiling. The computers are placed over the lines of supply openings so that cooled air flows through the computers. The computers discharge heated air from their upper-side grilles. The heat generation rate of the computers is set at 800 kcal/h per unit floor area (1 m^2 [10.8 ft^2]). The supply jet

velocity is assumed to be at 2 m/s (393.7 fpm) and the width of the supply opening is assumed to be 0.4 m (15.7 in.). The supply and exhaust openings alternate with each other, as is shown in Figure 1. The range of one flow unit formed by one supply opening is also shown in Figure 1. The flow and temperature fields are analyzed for a part of the room shown in Figure 1. The analyzed domain is one section of the room cut along the symmetrical plane of air distribution. Figure 2 shows detail of the flow fields analyzed.

In this study, physical quantities such as length, velocity, temperature, and so on, are often expressed in normalized values that are made dimensionless by dividing them by the representative values. The full-scale representative values used here are the width of the supply outlet A, L_o = 0.4 m (15.7 in.); the average velocity at the supply outlet A, U_o = 2 m/s (393.7 fpm); and the difference between the temperature at supply outlet A and the average overall exhaust inlet temperature, $\Delta\Theta_o$ = 15.0°C. Nondimensionalized temperature is expressed as the difference from that at supply outlet A, that is, the temperature at supply outlet A is shifted to zero.

EXPERIMENTS

Room Model

The experiments were carried out in a one-third scale model. The width of supply outlet A is set at 0.133 m in Figure 2. In this model, the air supply and exhaust rate can be controlled individually for each opening. The exterior of the model is insulated with 10-cm-thick plastic insulator. The inner side of the model is covered with stainless steel plates with a reflective surface in order to minimize the effects of radiant heat transfer.

The computer model is installed on the center supply outlet in the raised floor. The air that flows through this computer model is heated with an electric heater. The upper side of the computer model is covered with wire mesh and from this opening (hereafter called "opening B") heated air is discharged into the model room. The side walls of the computer model are insulated with 25-mm-thick glass wool insulator.

Similarities

Similarities of the model experiment must be considered, since a scale model is used ($n_l = L_{o,model}/L_{o,full\text{-}scale}$ = 1/3). In this experiment, the identical Ar number ($Ar = g\beta\Delta\Theta_o L_o/U_o^2$) is the only similarity considered between full-scale and scale model. The velocity scale in this experiment is the same ($n_v = U_{o,model}/U_{o,full\text{-}scale}$ = 1). Therefore, the scale temperature difference is three times full scale in the model experiment ($n_t = \Theta_{o,model}/\Theta_{o,full\text{-}scale}$ = 3) in order to ensure an identical Ar number ($n_t \cdot n_l/n_v^2$ = 1). The scale of the heat generation rate becomes one-third in the model experiment ($\because n_Q = n_l^2 \cdot n_v \cdot n_t$, here, $n_Q = Q_{o,model}/Q_{o,full\text{-}scale}$ = 1/3, Q_o = heat generation rate).

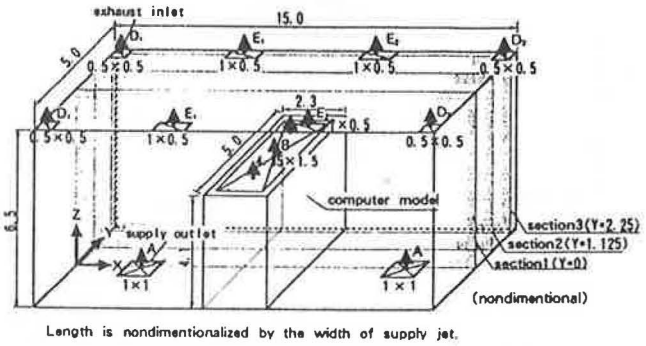

Figure 2 Flow field model analyzed. (Cut out area with three supply openings, see Figure 1.)

Measurement

The air velocity was measured with a three-dimensional ultrasonic anemometer with a short span (5 cm) and also with a thermistor anemometer. The temperature of both air and wall surface is measured with T-type (Cu-Co) thermocouples.

Velocity and Temperature Distribution at Supply Opening of Model

The supply jet generally has a great influence on the airflow and temperature distribution in the room. From the authors' experience, a discrepancy between the results of experiment and simulation is often due to a small difference in the supply jets. Detailed measurements of the model are required to ensure the same conditions in the simulation. Therefore, measurements of the velocity and temperature distributions at supply openings A and B were carried out in detail.

Figures 3 and 4 show the distribution of air velocity at supply opening A and distributions of air velocity and temperature at supply opening B. Air was heated by the computer model at opening B. Judging from these results, it is reasonable to conclude that the same uniform distributions of velocity and temperature are given at the boundary of the supply openings in the simulation.

CASES ANALYZED

The experimental conditions for each case analyzed are listed in Table 1, as are the conditions of the numerical simulation. Five cases were examined, with experiments conducted for all save Case 1-3. Case 1-1 is the only case without heat generation by the computer. Cases 1-1 and 1-2 are cases where supply and exhaust airflow rates are locally balanced in each flow unit, which is composed of the supply jet and the reverse flows surrounding it. Thus most of the supplied air for each opening is

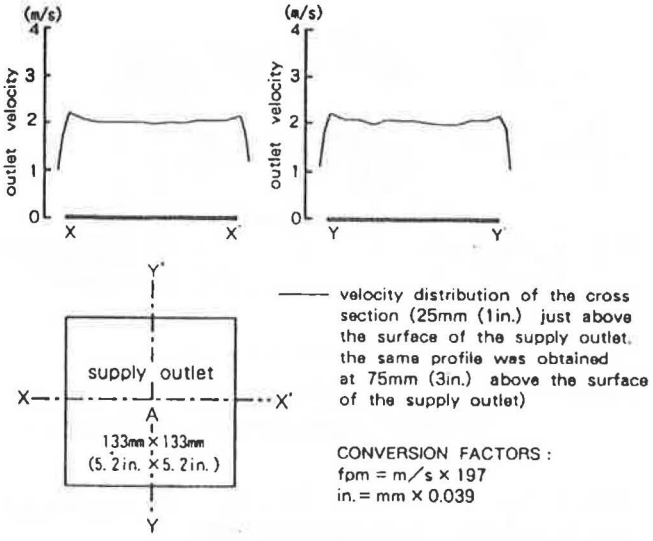

Figure 3 Velocity profiles of supply outlet A.

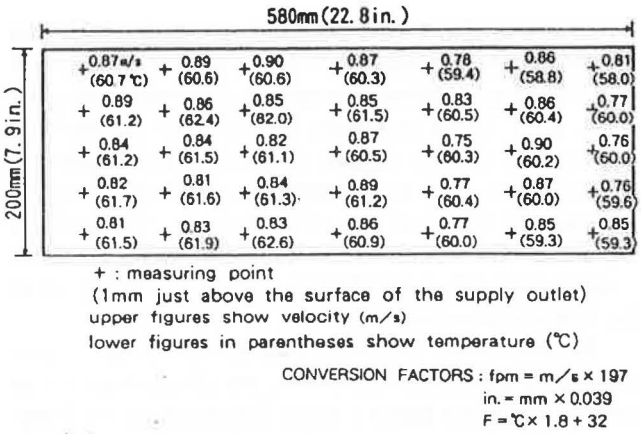

Figure 4 Velocity and temperature distribution at supply outlet B (upper surface of computer model).

exhausted from the exhaust inlets allotted to that flow unit. Cases 2 and 3 are cases where the airflow rates allotted to exhaust openings E_1 and E_2, just above the computer model, are increased/decreased in comparison with those of the other exhaust openings. In Case 4, the supply and exhaust airflow rates are made unequal by closing exhaust opening D_2. In this case, a large recirculating flow is formed within the whole room model.

NUMERICAL SIMULATION

Considering the bilateral symmetry in the Y-direction of the flow field shown in Figure 2, only half of the experimentally analyzed domain (from cross section 1 to the wall in Figure 2) is taken up for numerical analyses. The analyzed domain is discretized by a mesh system of 72(X) × 15(Y) × 23(Z) = 24,840.

Three-dimensional computations based on the k-ε two-equation turbulence model (Viollet type, Viollet 1987;

TABLE 1
Specifications for Cases Analyzed

item	Cases	1-1		1-2		1-3	2		3		4	
		E	S	E	S	S	E	S	E	S	E	S
supply outlet A	air volume (kg/h)	202	←	←	←	←	←	←	←	←	←	←
	velocity (m/s)	2.0	←	←	←	←	←	←	←	←	←	←
	temperature (℃)	–	–	26.9	←	←	←	←	←	←	←	←
supply outlet B	air volume (kg/h)	332	←	←	←	←	←	←	←	←	←	←
	velocity (m/s)	0.76	←	←	←	←	←	←	←	←	←	←
	temperature (℃)	–	–	63.0	←	←	←	←	←	←	←	←
exhaust inlet $D_1 \cdot D_2$	air volume (kg/h)	52	←	←	←	←	110	←	17	←	D_1 : 123 D_2 : 0	←
	temperature (℃)	–	–	31.6	30.4	30.2	36.2	36.0	29.2	27.7	D_1 : 39.5 D_2 : –	D_1 : 36.7 D_2 : –
	discharge of heat capacity (kcal/h)	–	–	230	173	163	980	960	40	10	D_1 : 680 D_2 : 0	D_1 : 580 D_2 : –
exhaust inlet $E_1 \cdot E_2$	air volume (kg/h)	132	←	←	←	←	75	←	167	←	E_1, E_2: 123	←
	temperature (℃)	–	–	45.8	47.9	48.1	52.4	53.5	42.9	44.6	E_1 : 54.8 E_2 : 36.0	E_1 : 56.6 E_2 : 35.9
	discharge of heat capacity (kcal/h)	–	–	2410	2670	2700	1830	1920	2570	2840	E_1 : 1640 E_2 : 540	E_1 : 1750 E_2 : 530
difference of temperature between exhaust and supply (℃)		–	–	14.9	16.1	16.2	15.9	16.1	14.7	16.2	16.2	16.2
Ar number ($\times 10^{-2}$)		–	–	1.86	2.02	2.03	2.00	2.03	1.86	2.03	2.05	2.03
amount of inner heat generator (kcal/h)		–	–	2880	←	←	←	←	←	←	←	←

note E : experiment, S : simulation

CONVERSION FACTORS : F = ℃ × 1.8 + 32
fpm = m/s × 197
lb./h = kg/h × 2.2

Murakami et al. 1991) are conducted. The basic equations are listed in Table 2. Boundary conditions used are shown in Table 3 (Launder and Spalding 1974; Murakami et al. 1991).

Conditions of numerical simulations correspond exactly to those of the experiments, as shown in Table 1. Case 1-3 is added in the simulation. In this case, the boundary conditions of the vertical walls are different from the others—in order to analyze the effects of the presence or lack of solid walls in the cut model, the boundary conditions are changed from solid walls to free slip conditions for a symmetrical plane of the flow field.

RESULTS OF EXPERIMENTS AND NUMERICAL SIMULATIONS

Case 1-1: Locally Balanced Supply and Exhaust Airflow without Heat Generation

Velocity vectors at each measuring cross section in Case 1-1 are shown in Figure 5. Since the resulting flow fields of both the experiment and the simulation are exactly symmetrical, only the left half of the sectional plane is shown. Vertical profiles of the scalar velocity (resultant velocity) distribution are shown in Figure 6. Figure 6 also shows the scalar velocity distributions of Case 1-2 (with heat generation) in order to compare the two cases with respect to the effect of the buoyant heated air discharged from the computer model.

The numerical simulation generally corresponds with the model experiment for the velocity vector field. The jets from floor supply outlet A move toward the ceiling and spread horizontally. The flows that reach the walls form downward streams (Figure 5(1), (2), (3)). Some parts of the diverging flows along the ceiling collide with the counterflows discharged from outlet B of the computer model, and then they form downward flows as well. However, some of them form a little recirculating flow under the ceiling (Figure 5(1)). Judging from the total flow field in the model room, each flow area allotted to one supply jet can be modeled as a flow unit, a typical model of which consists of a supply jet and the surrounding reverse flows. Thus the total flow patterns in the room can be modeled as a serial combination of such flow units.

In the simulation, the diverging flows along the ceiling slip into the space between the counterflows and the ceiling (Figure 5(1)-(b), (2)-(b)). When the diverging flows along the ceiling reach the corner of each flow unit, some of them are smoothly exhausted through the exhaust inlets in the ceiling (Figure 5(3)).

Generally, the results of the simulation correspond to the observed flow pretty well. However, some discrepancy between them is observed near the side wall. While a strong downward flow along the wall (Figure 5(1), (2), (3), $X = 0.3$) is observed in the experiment, the simulated downward flow is weak.

TABLE 2
k-ε Model Equations (Viollet Type)

$$\frac{\partial U_i}{\partial x_i} = 0 \tag{1}$$

$$\frac{DU_i}{Dt} = -\frac{1}{\rho}\frac{\partial}{\partial x_i}\left[P+\frac{2}{3}k\right] - \frac{\partial}{\partial x_j}\left[\nu_t\left(\frac{\partial U_i}{\partial x_j}+\frac{\partial U_j}{\partial x_i}\right)\right] - g_i \cdot \beta \cdot \Theta \tag{2}$$

$$\frac{Dk}{Dt} = \frac{\partial}{\partial x_j}\left[\frac{\nu_t}{\sigma_k}\frac{\partial k}{\partial x_j}\right] + P_k + G_k - \varepsilon \tag{3}$$

$$\frac{D\varepsilon}{Dt} = \frac{\partial}{\partial x_j}\left[\frac{\nu_t}{\sigma_\varepsilon}\frac{\partial \varepsilon}{\partial x_j}\right] + \frac{\varepsilon}{k}(C_{\varepsilon 1}P_k + C_{\varepsilon 3}G_k - C_{\varepsilon 2}\varepsilon) \tag{4}$$

$$\frac{D\Theta}{Dt} = \frac{\partial}{\partial x_j}\left[\frac{\nu_t}{\sigma_\theta}\frac{\partial \Theta}{\partial x_j}\right] \tag{5}$$

$$P_k = \nu_t\left(\frac{\partial U_i}{\partial x_j}+\frac{\partial U_j}{\partial x_i}\right)\frac{\partial U_i}{\partial x_j} \tag{6}$$

$$G_k = g_i \cdot \beta \cdot \frac{\nu_t}{\sigma_\theta}\cdot\frac{\partial \Theta}{\partial x_i}\cdot\delta_{i3} \tag{7}$$

$$\nu_t = C_\mu \cdot \frac{K^2}{\varepsilon} \tag{8}$$

$C_{\varepsilon 1}$:1.44 $C_{\varepsilon 2}$:1.92 σ_k:1.0 σ_ε:1.3 σ_θ:1.0 C_μ:0.09

$C_{\varepsilon 3}$: $G_k > 0$ $C_{\varepsilon 3}$=1.44, $G_k \leqq 0$ $C_{\varepsilon 3}$=0.0

TABLE 3
Boundary Conditions

(1) Supply outlet boundary
 ①Supply outlet A
  U_N=2.0(m/s), U_T=0.0(m/s), k_A=0.005(m^2/s^2)
  $\varepsilon = C_\mu \cdot k^{3/2}/\ell$, θ_A=26.9(℃), ℓ=0.001(m)
 ②Supply outlet B
  U_N=0.68(m/s), U_T=0.0(m/s), k_B=0.0003(m^2/s^2)
  $\varepsilon = C_\mu \cdot k^{3/2}/\ell$, θ_B=63.0(℃), (Case1-1 : θ_B=26.9℃), ℓ=0.001(m)
(2) Exhaust inlet boundary
 Case 1-1, 1-2, 1-3 : U_D=2.71(m/s), U_E=3.52(m/s)
 Case 2 : U_D=5.79(m/s), U_E=1.98(m/s)
 Case 3 : U_D=0.90(m/s), U_E=4.44(m/s)
 Case 4 : U_{D1}=6.47(m/s), U_{D2}=0.0(m/s), $U_{E1,E2}$=3.26(m/s), U_T=0.0(m/s)
 Case 1-1, 1-2, 1-3, 2, 3, 4 : k=free slip, ε=free slip, θ=free slip
(3) Wall boundary
 U_N=0.0(m/s), U_T(log law) : $U_{T1}(C_\mu^{1/2}k)^{1/2}/(\tau/\rho) = 1/\kappa \cdot \ell_n(E \cdot h_1(C_\mu^{1/2}k)^{1/2}/\nu)$
 $\partial k/\partial Z$=0.0, ε_1 term in k equation : $\varepsilon_1 = \varepsilon \cdot \ell_n(E \cdot h_1(C_\mu^{1/2}k)^{1/2}/\nu)$
 $\varepsilon = (C_\mu \cdot k^{3/2})/(C_\mu^{1/4}\kappa \cdot h_1)$
 (Case1-3 : U, k, ε, θ : free slip)
 h : length from the wall surface to the near-wall node
 E : 9.0, constant of the wall roughness (for a smooth wall)
 ν : 1/Re, kinematic viscosity
 κ : 0.4, von karman constant
(4) Finite difference scheme
 Time marching : adams bashforth scheme
 Convective term : upwind scheme
suffix N : normal component, T : tangential component
 A, B : supply outlet A, B D, E : exhaust inlet D, E

Calulations are conducted with physical dimension.
CONVERSION FACTORS : fpm = m/s × 197
in. = m × 39

Generally good agreement between the simulations and experiments is observed for the vertical distribution of scalar velocity. A rather large discrepancy between them is observed in the area where the jet from supply opening A is mixed with the surrounding room air (Figure 6(1), $X = 4.2$) and in the area near the wall where downward flow is observed (Figure 6(1) $X = 0.3$, (2) $X = 0.3$). In the simulation, the maximum deviation from the experimental result here is as much as 20% of the supply jet velocity; however, in the other areas, the difference does not exceed 10%.

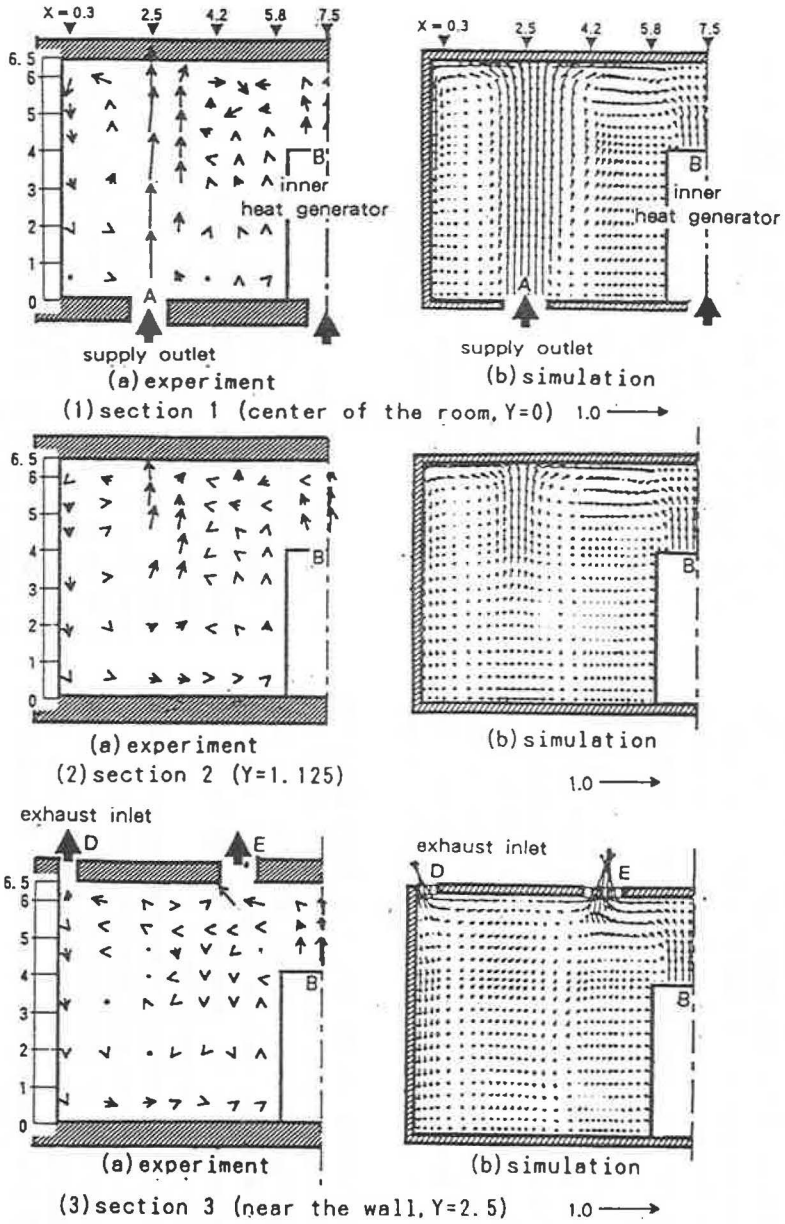

Figure 5 *Velocity vectors in Case 1-1*
(1) section 1 (center of the room, Y = 0) (a) experiment (b) simulation
(2) section 2 (Y = 1.125) (a) experiment (b) simulation
(3) section 3 (near the wall, Y = 2.5) (a) experiment (b) simulation.

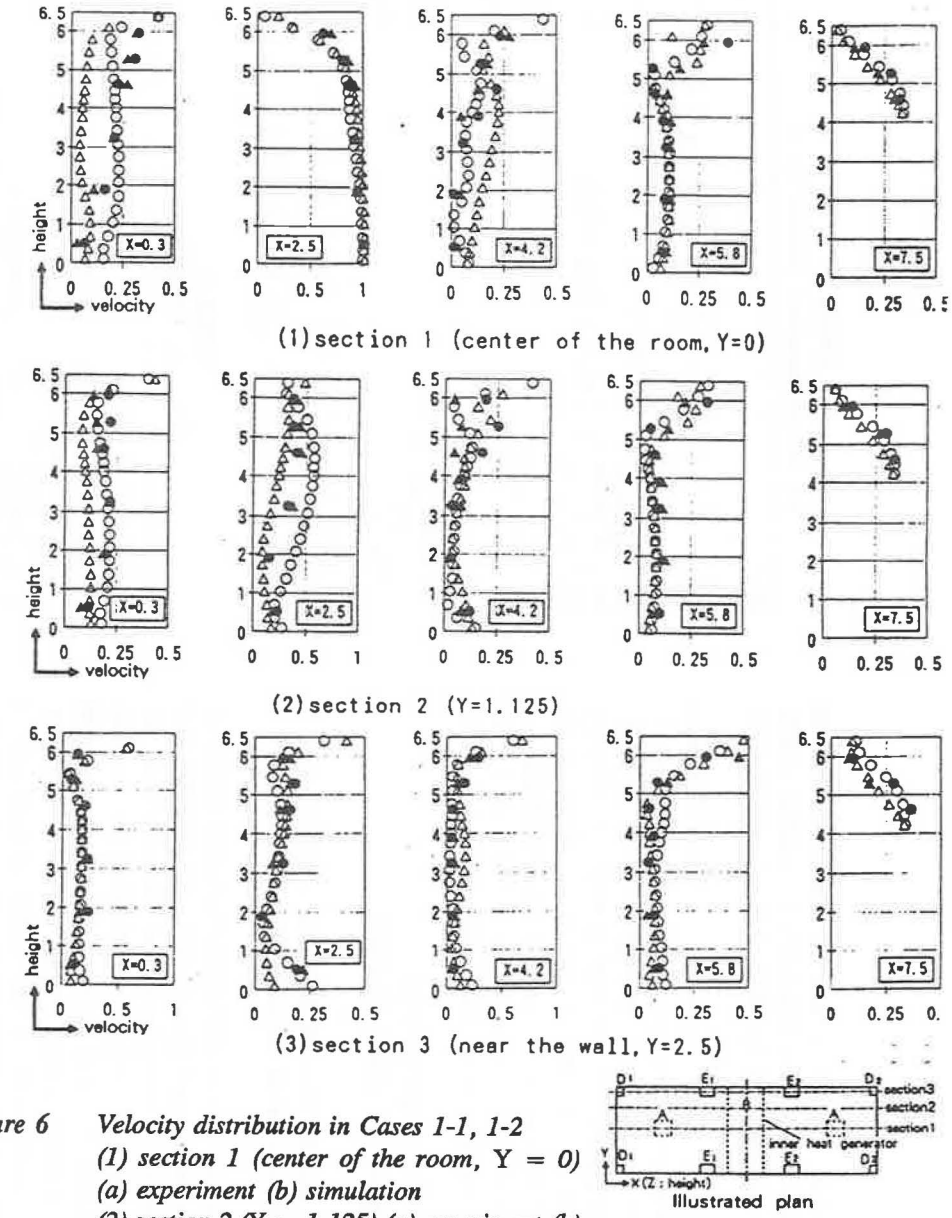

Figure 6 *Velocity distribution in Cases 1-1, 1-2*
(1) section 1 (center of the room, Y = 0) (a) experiment (b) simulation
(2) section 2 (Y = 1.125) (a) experiment (b) simulation
(3) section 3 (near the wall, Y = 2.5) (a) experiment (b) simulation.

Cases 1-2 and 1-3: Locally Balanced Supply and Exhaust Airflow with Heat Generation

Velocity Fields Velocity vectors and the distributions of scalar velocity for Case 1-2 are shown in Figures 7 and 8. In this case, the supply and exhaust airflow rates are the same as those in Case 1-1; the only different condition is heat generation.

Figure 7 shows that the results of the numerical simulation correspond well with the observed results. The jets from supply openings A (floor) and B (top of the computer model) hit the ceiling and then spread horizontally. The diverging flows along the ceiling reach the walls and then form downward flows, which collide with each other. After the collision, they form a recirculating flow larger than that of Case 1-1 (Figure 7(1), (2)). In the presence of heat generation (Case 1-2), the jet from opening B of the model computer becomes stronger due to the buoyancy effect, which consequently makes the recirculating flows larger than in the case of no heat generation (Case 1-1, in Figure 5(1), (2)). Little difference between Case 1-1 and Case 1-2 is observed in the patterns of the velocity vectors except for the recirculating flows, since the air exchange rate of the room is so high that the Ar number of the buoyant jet from the computer model is small. It may be concluded that the influence of buoyancy is slight and that the major flow pattern is well modeled as a serial combination of local flow units.

Figure 8 shows that correspondence between the simulations and the experiment is greatly improved in Case 1-2 and 1-3 compared with Case 1-1 (without heat generation). Figure 6 shows results both with and without heat generation. The experimental results for the two cases show little difference; however, the simulations of the two cases differ from each other to a certain degree near the wall (Figure 6(1), $X = 0.3$; (2), $X = 0.3$ and $X = 2.5$). The reason for this discrepancy is not clear; however, it is probable that some errors are due to the inadequacy of the turbulence model used here. On the whole, it may be concluded that the influence of buoyancy can hardly be observed in the major flow pattern except for the small recirculating flow mentioned above. As shown in Figure 8, for Case 1-3, all vertical boundary planes are assumed to be symmetrical, whereas in Case 1-2 the analyzed domain is assumed to be enclosed by solid walls. Comparing Case 1-2 with Case 1-3, little difference is observed in the scalar velocity distribution. However, several differences are observed in the distribution of turbulent kinetic energy, k, and the dissipation rate of turbulent energy, ε. (Figures of the distribution of k and ε are omitted.) With regard to velocity distribution, the experimental model with solid walls set at the symmetrical plane of the flow fields has little error.

Temperature Fields The isothermal contour lines and vertical temperature distribution of each cross section are shown in Figures 9 and 10.

Figure 9 shows that the heat discharged from the computer model is convected by the airflow and spreads out above the computer model but does not diffuse throughout the whole space.

The temperature distribution obtained from the numerical simulation corresponds well with the experimental one except for the area just above the computer model (Figure 10(1), $X = 7.5$; (2), $X = 7.5$; and (3), $X = 7.5$). Temperature is very high above the heat discharge opening in the simulation, whereas in the experiment, temperature becomes rather low near the ceiling at the same position since the cooled air from supply opening A slips into the space. One possible reason for this discrepancy is that in the numerical simulation, the horizontally spreading flow along the ceiling from supply jet A is weaker than the flow observed in the experiment (Figure 8(1), $X = 2.5$, $X = 4.2$, $X = 5.8$). This phenomenon might suggest that the wall boundary condition at the ceiling is not modeled adequately and the numerical simulation is thus not able to exactly reproduce this slipping flow. Another possible factor might be shortcomings in the turbulence model with regard to the turbulent transport of heat. The k-ε model is based on the eddy viscosity model, but this model may have significant errors in anisotropic turbulent heat transportation (Murakami et al. 1991). The latter factor should be investigated further using some more elaborate turbulence model, such as the differential second moment closure model. However, the present simulation predicts the entire temperature field to a sufficient degree, and the difference from the measured value does not exceed 20% of the representative temperature difference, $\Delta\Theta_o$, at most measuring points.

A comparison between Case 1-2 and Case 1-3 is shown in Figure 10; differences are hardly observable in the temperature distribution. The model with adiabatic solid walls set at the symmetrical plane of the flow field has little error.

In Case 1-2, where supply and exhaust airflow rates are locally balanced in each flow unit, about 91% of the heat is exhausted through the openings of E_1 and E_2. That is, the heat ratio exhausted by the inlet belonging to the same flow unit in which heat is discharged is 91%, and only 9% of the heat is transported to other flow units. Thus, the locally balanced supply and exhaust airflow ventilation system is sufficiently effective in exhausting the heat discharged into the room.

Case 2: Decreasing Exhausting Airflow Rate in Heat Discharged Flow Unit

Velocity Fields Velocity vectors and vertical distribution of scalar velocity at each section for Case 2 are shown in Figures 11 and 12.

The results of the numerical simulation, as in other cases, generally correspond with those of the model

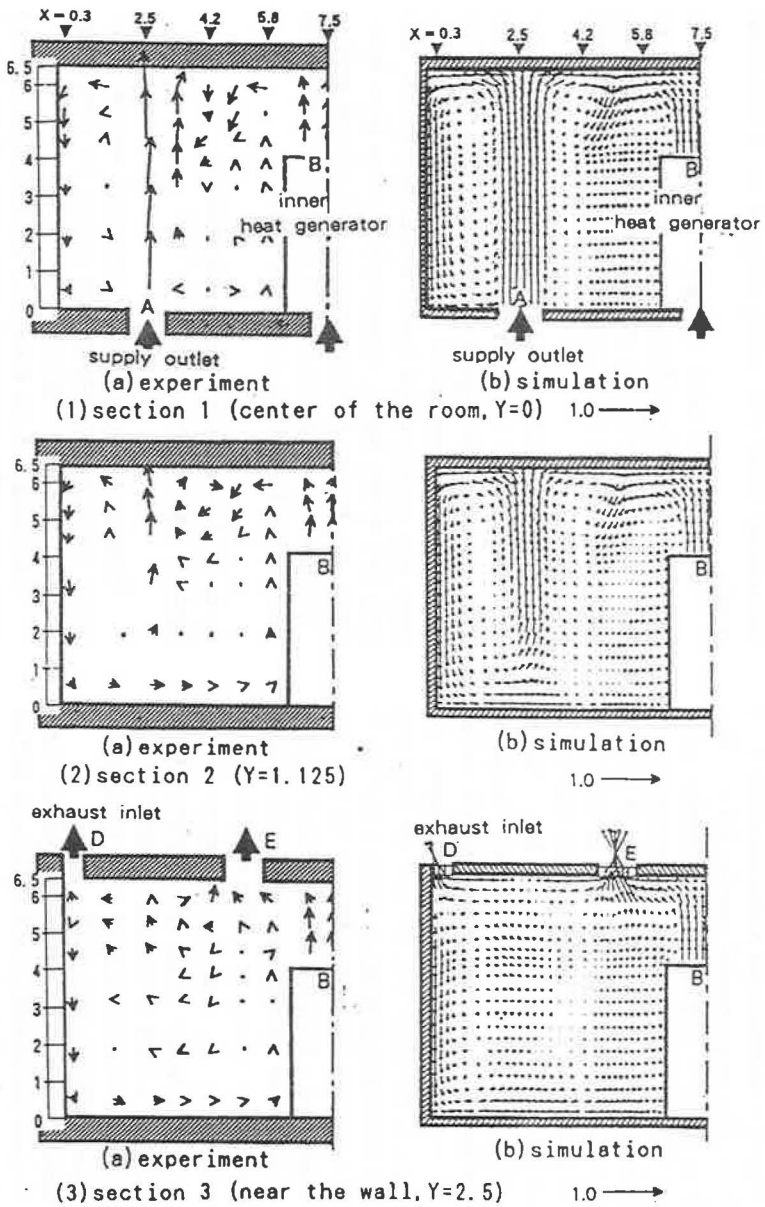

Figure 7 *Velocity vectors in Case 1-2*
(1) section 1 (center of the room, Y = 0) (a) experiment (b) simulation
(2) section 2 (Y = 1.125) (a) experiment (b) simulation
(3) section 3 (near the wall, Y = 2.5) (a) experiment (b) simulation.

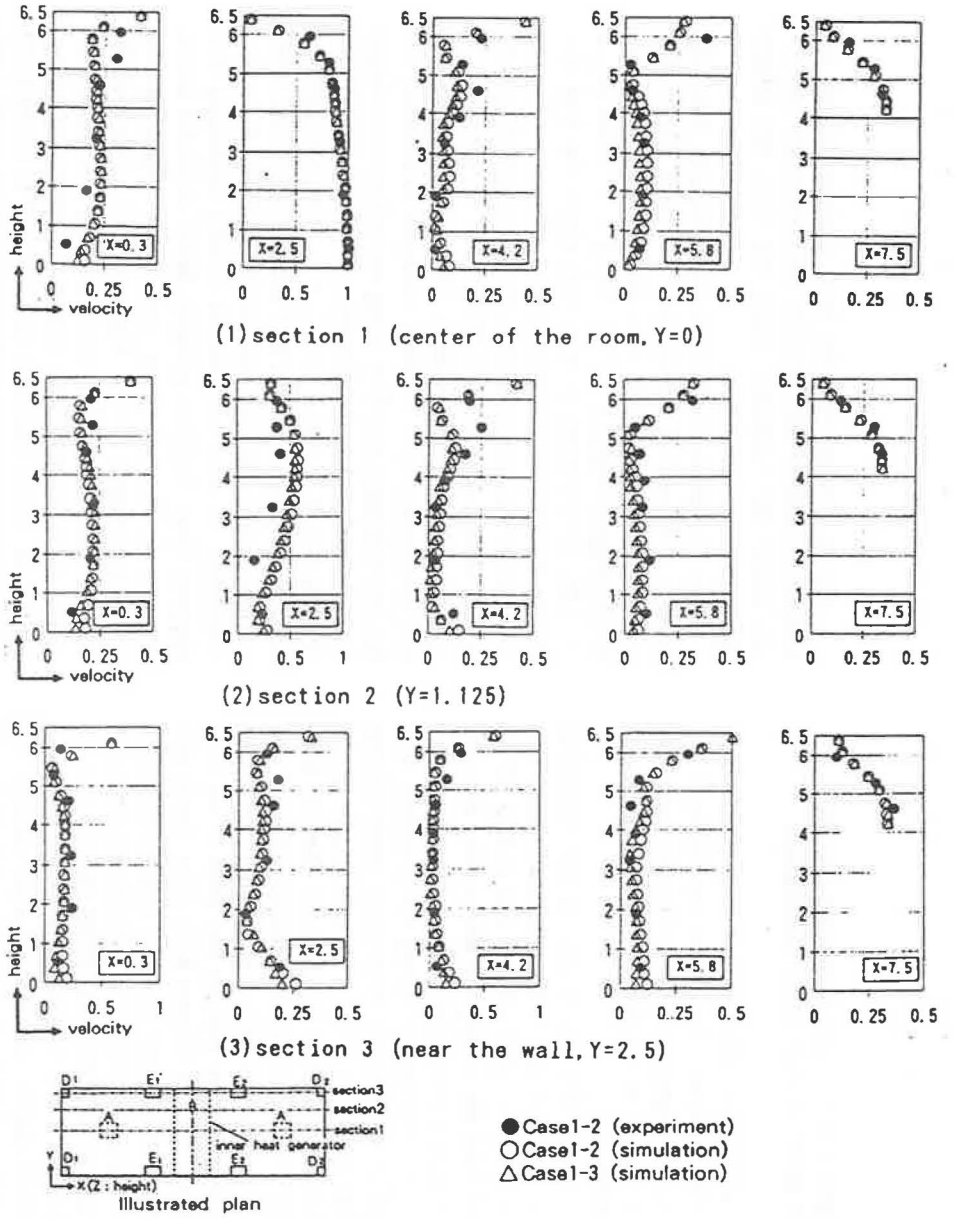

Figure 8 *Velocity distribution in Cases 1-2, 1-3*
(1) section 1 (center of the room, Y = 0) (a) experiment (b) simulation
(2) section 2 (Y = 1.125) (a) experiment (b) simulation
(3) section 3 (near the wall, Y = 2.5) (a) experiment (b) simulation.

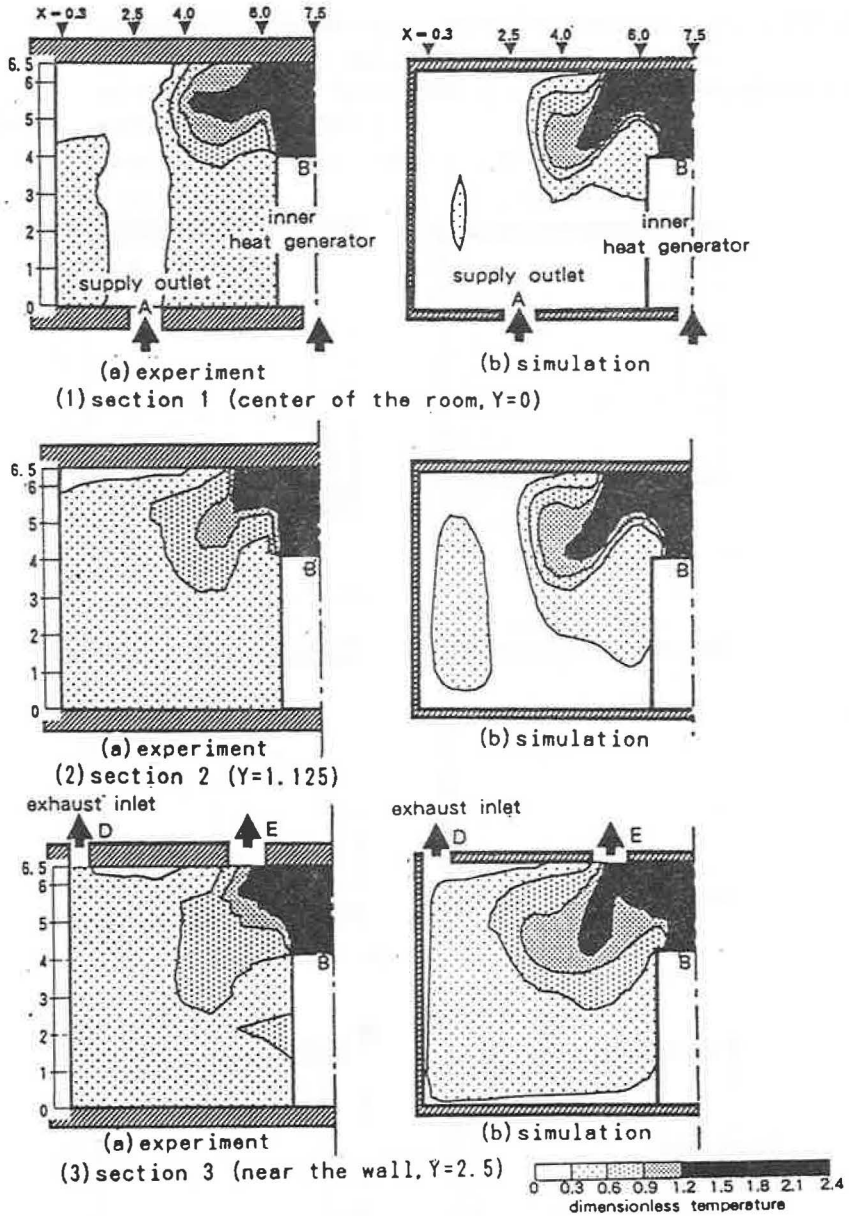

Figure 9 *Temperature distribution in Case 1-2*
(1) section 1 (center of the room, Y = 0) (a) experiment (b) simulation
(2) section 2 (Y = 1.125) (a) experiment (b) simulation
(3) section 3 (near the wall, Y = 2.5) (a) experiment (b) simulation.

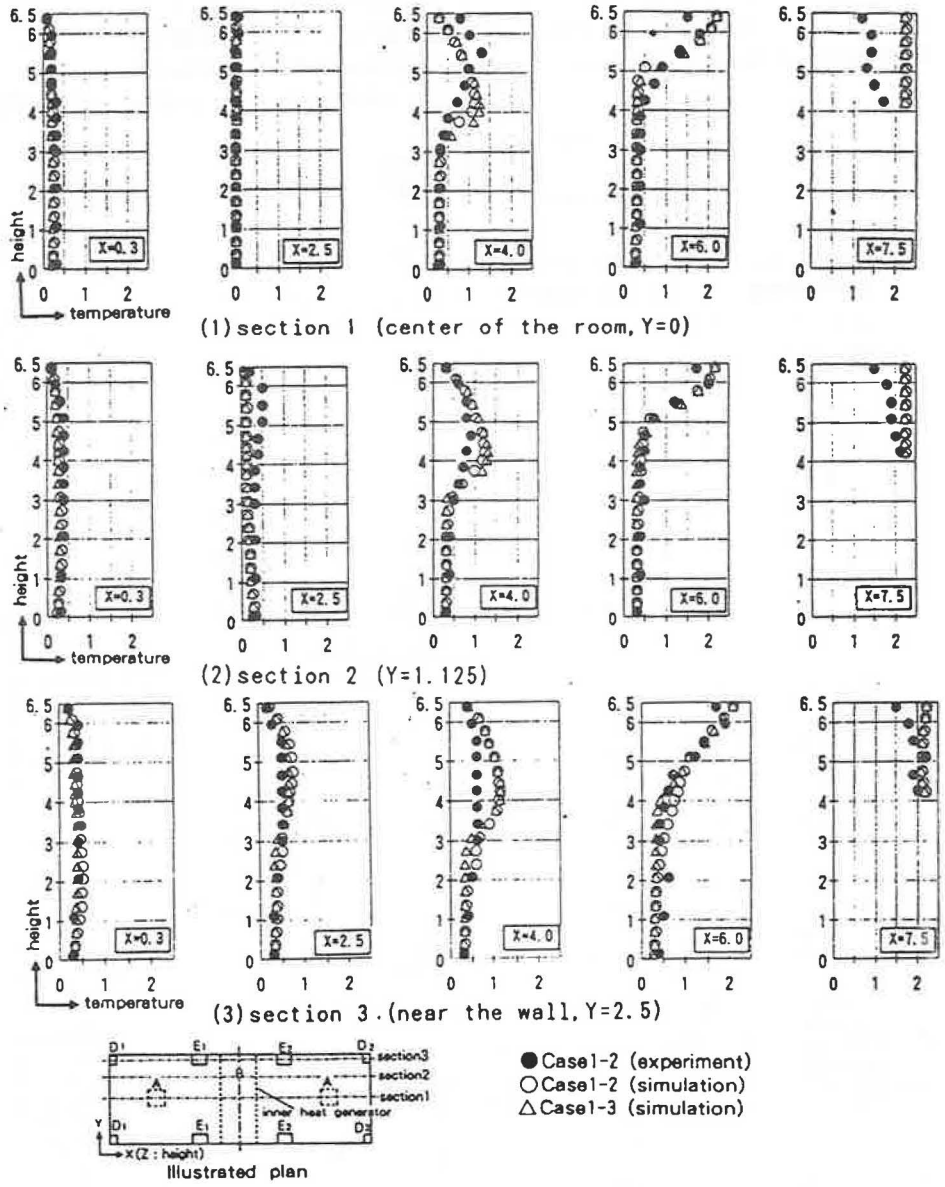

Figure 10 *Temperature distribution in Cases 1-2, 1-3*
(1) section 1 (center of the room, Y = 0) (a) experiment (b) simulation
(2) section 2 (Y = 1.125) (a) experiment (b) simulation
(3) section 3 (near the wall, Y = 2.5) (a) experiment (b) simulation.

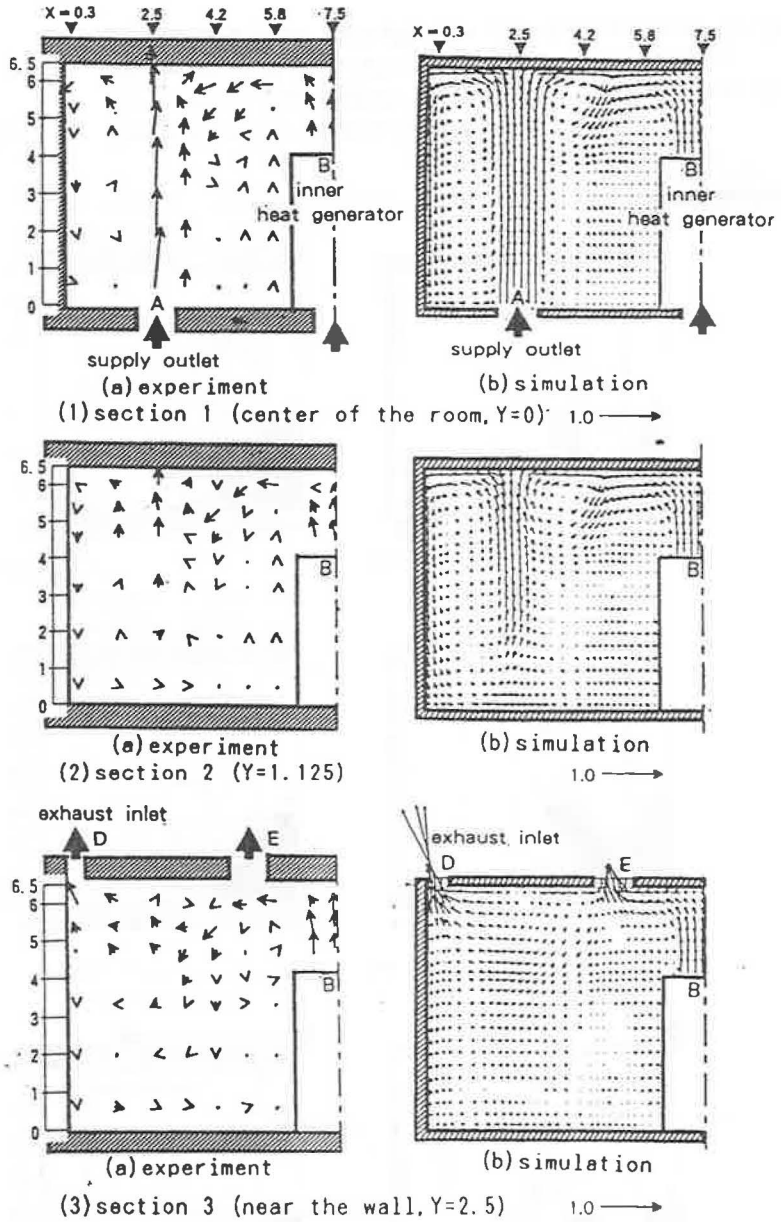

Figure 11 *Velocity vectors in Case 2*
(1) section 1 (center of the room, Y = 0) (a) experiment (b) simulation
(2) section 2 (Y = 1.125) (a) experiment (b) simulation
(3) section 3 (near the wall, Y = 2.5) (a) experiment (b) simulation.

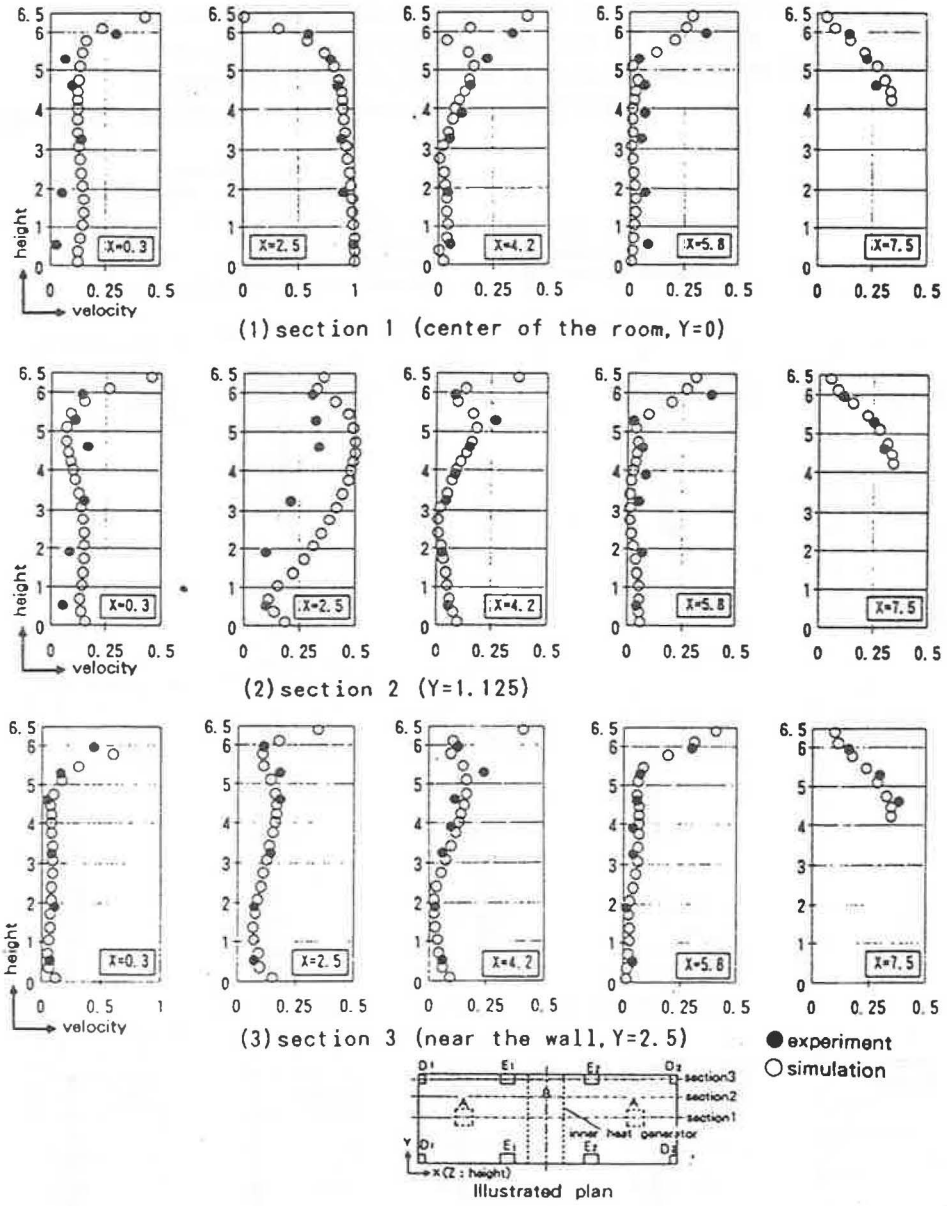

Figure 12 *Velocity distribution in Case 2*
(1) section 1 (center of the room, Y = 0) (a) experiment (b) simulation
(2) section 2 (Y = 1.125) (a) experiment (b) simulation
(3) section 3 (near the wall, Y = 2.5) (a) experiment (b) simulation.

experiment for velocity vectors. Moreover, the airflow pattern of Case 2 is almost the same as that in Case 1-2. It is difficult to differentiate among the airflow patterns of Case 1-2, Case 2, and Case 3 (Figures 7, 11, and 15).

Generally good correspondence between the numerical simulation and the model experiment is observed for the vertical distribution of scalar velocity. However, at point $X = 2.5$ in cross section 2, which is located at the side of supply opening A, the values of scalar velocity obtained from the numerical simulation are 20% to 50% higher than the experimental values (Figure 12(2)). In the region where the discrepancy is observed, the supply jet mixes with the surrounding air, and velocity distribution changes rapidly in the horizontal direction. Thus a small difference in measuring points causes a large difference in measured velocity. Perhaps the reason for the discrepancy is not attributable only to errors in the numerical simulation.

Temperature Fields Figures 13 and 14 show the isothermal contour lines and vertical temperature distribution.

As shown in Figure 14, the temperature above the computer model obtained in the model experiment ($X = 7.5$ in Figures 14(1), (2), and (3)) is a little lower than that in the numerical simulation, as well as that in Case 1-2. In Case 2, however, the difference between the simulation and the experiment is smaller than in Case 1-2. In the experiment, the temperature above the computer model rises significantly in comparison with Case 1-2, and this causes less difference between the simulation and the experiment.

Comparing Case 1-2 and Case 2, although almost the same pattern of velocity vectors is found, the temperature fields are completely different in the two cases. On the whole, temperature values of the room in Case 2 are higher than those in Case 1-2 due to the reduction of the exhaust airflow rate in the flow unit where heat is discharged. The difference between supply and exhaust airflow rates within the flow unit produces overflows into other flow units, and part of the discharged heat is convected toward other spaces. The ratio of heat exhausted from exhaust opening E, which corresponds to the exhaust openings of the flow unit formed by the air discharged from the computer model, is only 63% of the heat discharged into the room. The rest of the heat is exhausted from exhaust opening D, which accounts for more than 34%, about four times more than Case 1-2.

Case 3: Increasing Exhausting Airflow Rate in Heat Discharged Flow Unit

Velocity Fields Velocity vectors and distributions of scalar velocity for Case 3 are shown in Figures 15 and 16.

The results of the numerical simulation agree very well with those of the experiment. Moreover, the airflow pattern of Case 3 is exactly the same as that of Case 1-2. It is difficult to find any difference in airflow patterns among Case 1-2, Case 2, and Case 3 (Figures 7, 11, and 15).

Temperature Fields Figures 17 and 18 compare the experiment and the numerical simulation in terms of isothermal contour lines and vertical temperature distribution.

As shown in Figure 18, the temperature above the computer model given by the model experiment ($X = 7.5$ in Figures 18(1), (2), and (3)) is lower than that of the numerical simulation, as well as that of Case 1-2. In Case 3, the difference between the simulation and the experiment shows the same tendency as Case 1-2. Except for this apparent discrepancy, the numerical simulation reproduces the temperature fields observed in the experiment with sufficient accuracy. As shown in Figure 17, the experiment gives a rather wider range for $\Delta\Theta > 0.9$, so the numerical simulation predicts a rather less diffuse field of temperature. This difference may be due to shortcomings in the eddy viscosity model for turbulence diffusion.

The airflow rates allotted to exhaust opening E, which is located just above the model computer, are increased in Case 3, so the heat discharged into the room is immediately exhausted without diffusing throughout the room. The ratio of exhausted heat from exhaust opening E accounts for about 98% of the heat discharged into the room. That is, only 2% of the heat is convected and transported into other flow units. It may be concluded that this system is highly efficient in exhausting the heat discharged within the room.

Case 4: Large Circulating Flow in Room

In Case 4, the exhaust D_2 of the right-side flow units is closed, creating a general airflow pattern moving from the right to the left side.

Velocity Fields Figure 19 shows the velocity vectors and the scalar velocity of Case 4. The scalar velocity of the experiment and that of the numerical simulation correspond well with each other, on the whole.

The air discharged from the computer model inclines to the left in both experiment and numerical simulation. This is caused by the asymmetrical condition of the exhaust.

Temperature Fields Figure 20 compares the experiment and the numerical simulation in terms of isothermal contour lines and the vertical temperature distribution.

As in the other cases, there is a tendency for the numerical simulation to predict higher temperatures above the model computer (at $X = 7.5$ in the center area of section 1) than are observed in the experiment (Figure 20(1)). Also, at $X = 4.0$ and 6.0 in the circulating flow to the left of the computer model, the numerical simula-

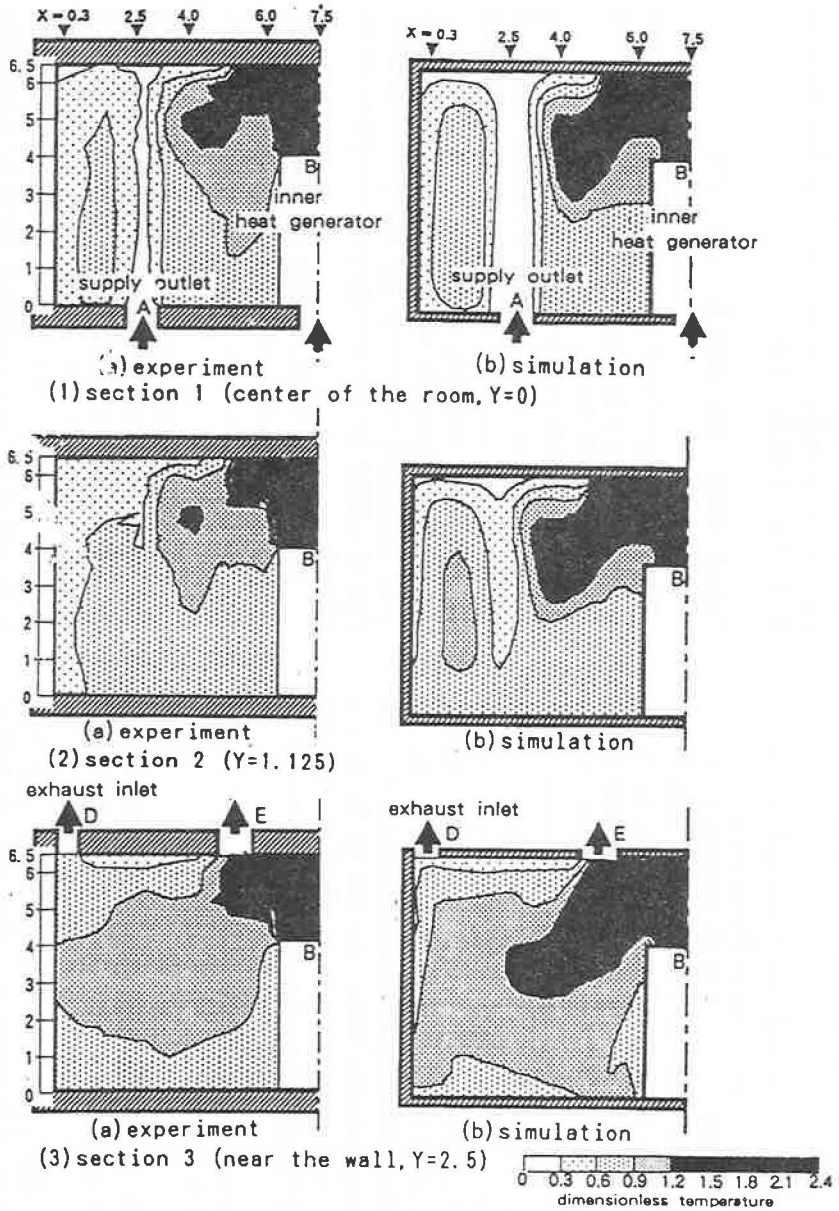

Figure 13 *Temperature distribution in Case 2*
(1) section 1 (center of the room, Y = 0) (a) experiment (b) simulation
(2) section 2 (Y = 1.125) (a) experiment (b) simulation
(3) section 3 (near the wall, Y = 2.5) (a) experiment (b) simulation.

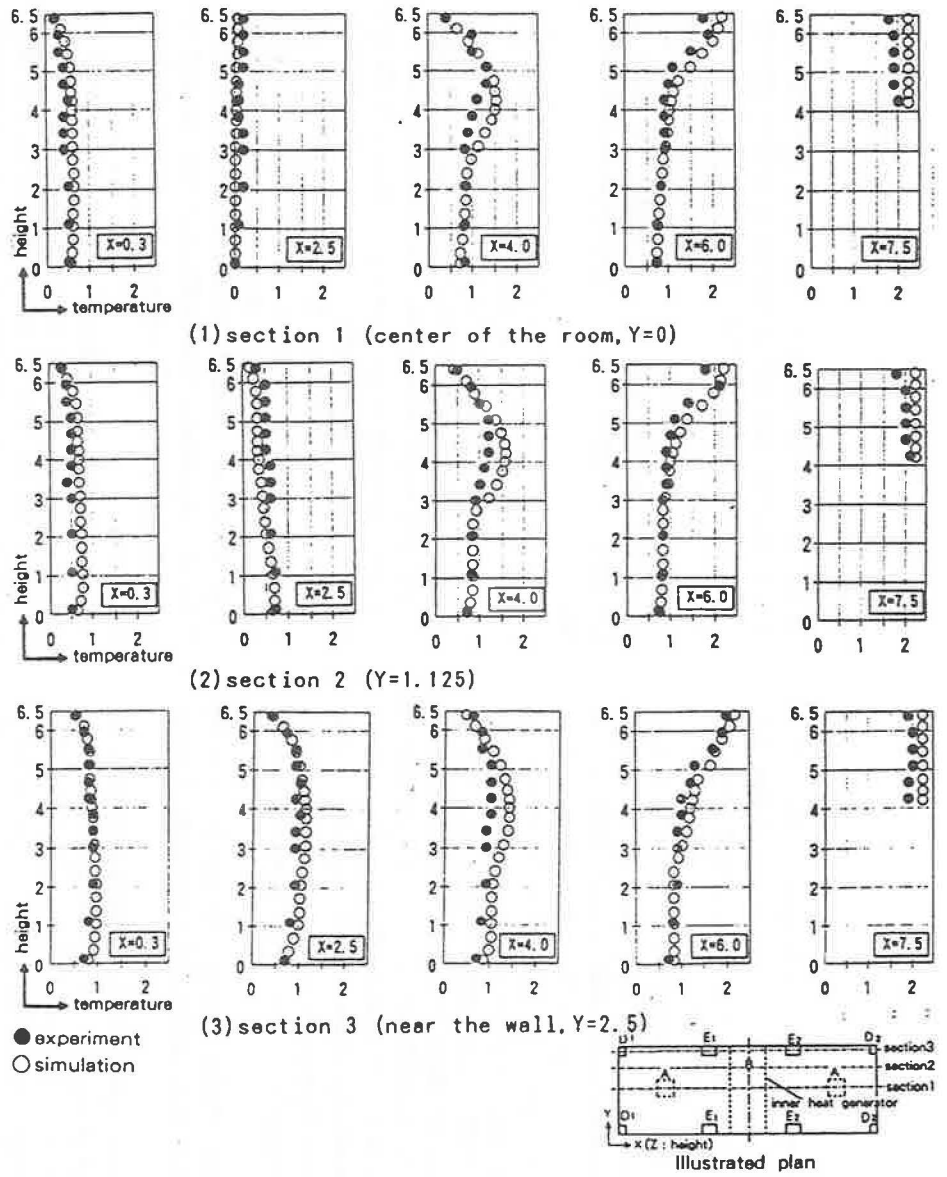

Figure 14 *Temperature distribution in Case 2*
(1) section 1 (center of the room, Y = 0) (a) experiment (b) simulation
(2) section 2 (Y = 1.125) (a) experiment (b) simulation
(3) section 3 (near the wall, Y = 2.5) (a) experiment (b) simulation.

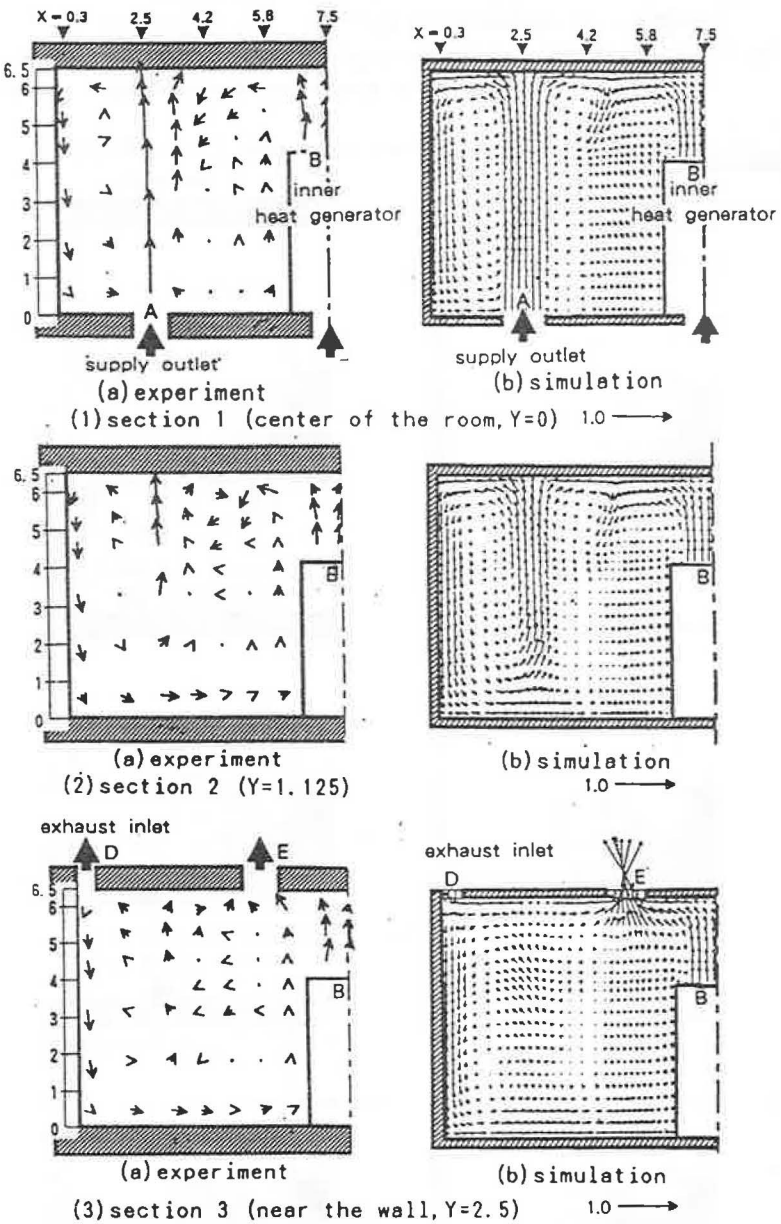

Figure 15 *Velocity vectors in Case 3*
(1) section 1 (center of the room, Y = 0) (a) experiment (b) simulation
(2) section 2 (Y = 1.125) (a) experiment (b) simulation
(3) section 3 (near the wall, Y = 2.5) (a) experiment (b) simulation.

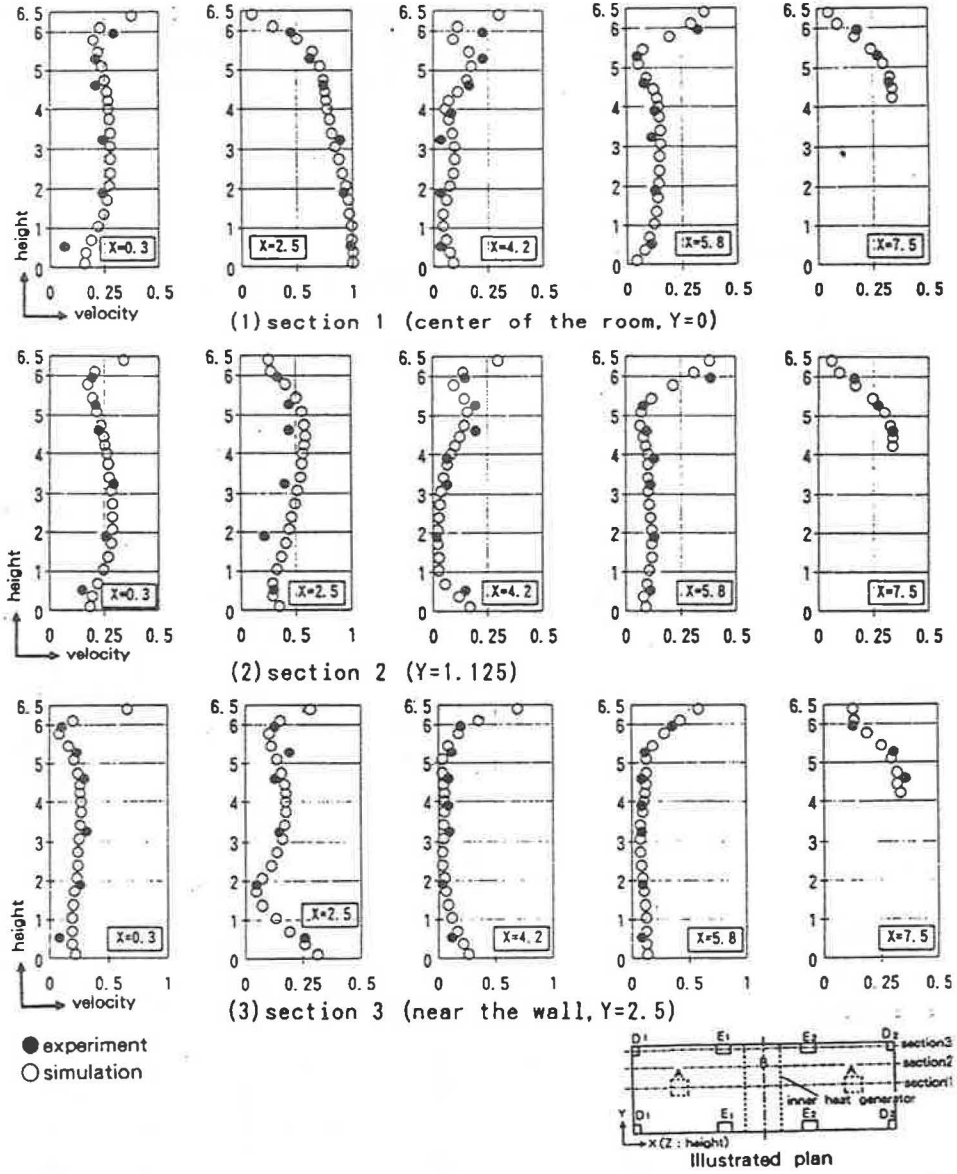

Figure 16 *Velocity distribution in Case 3*
(1) section 1 (center of the room, Y = 0) (a) experiment (b) simulation
(2) section 2 (Y = 1.125) (a) experiment (b) simulation
(3) section 3 (near the wall, Y = 2.5) (a) experiment (b) simulation.

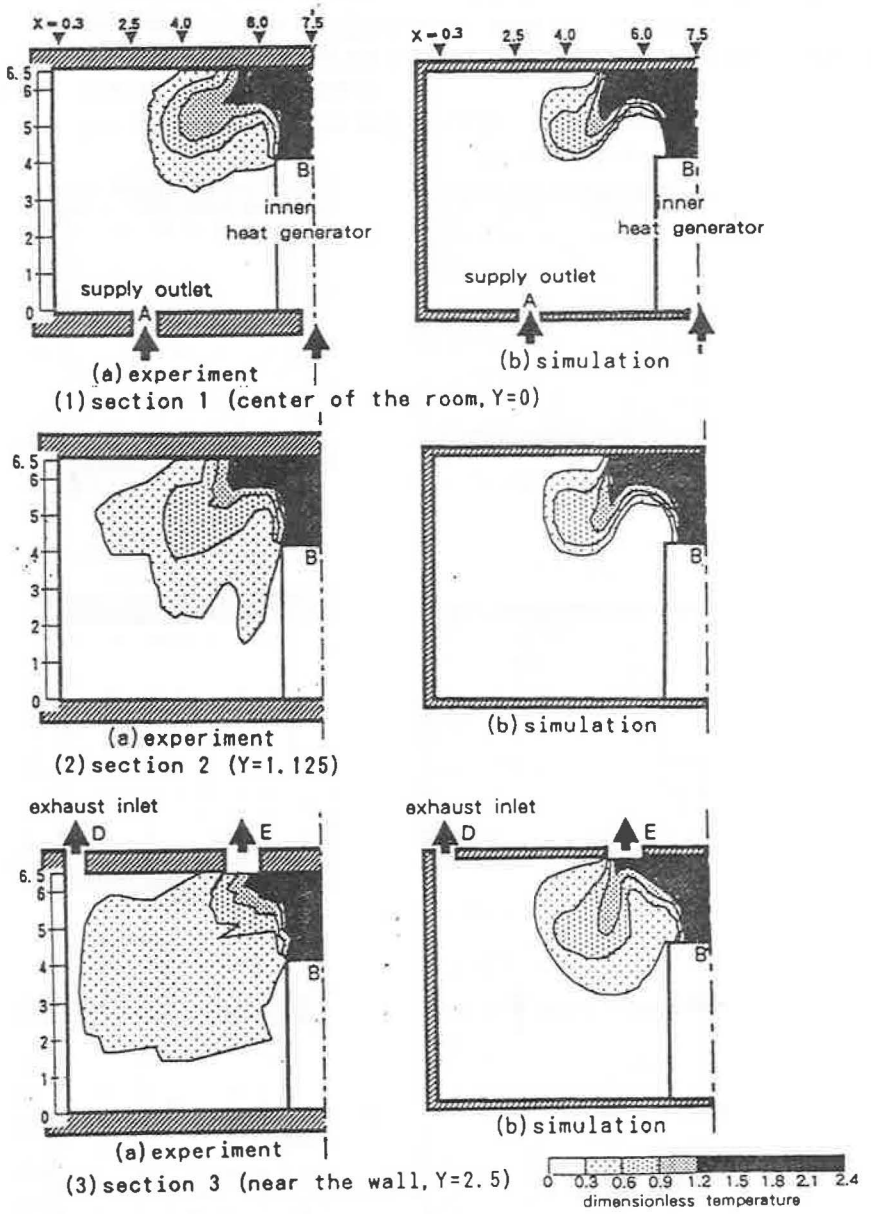

Figure 17 *Temperature distribution in Case 3*
(1) section 1 (center of the room, Y = 0) (a) experiment (b) simulation
(2) section 2 (Y = 1.125) (a) experiment (b) simulation
(3) section 3 (near the wall, Y = 2.5) (a) experiment (b) simulation.

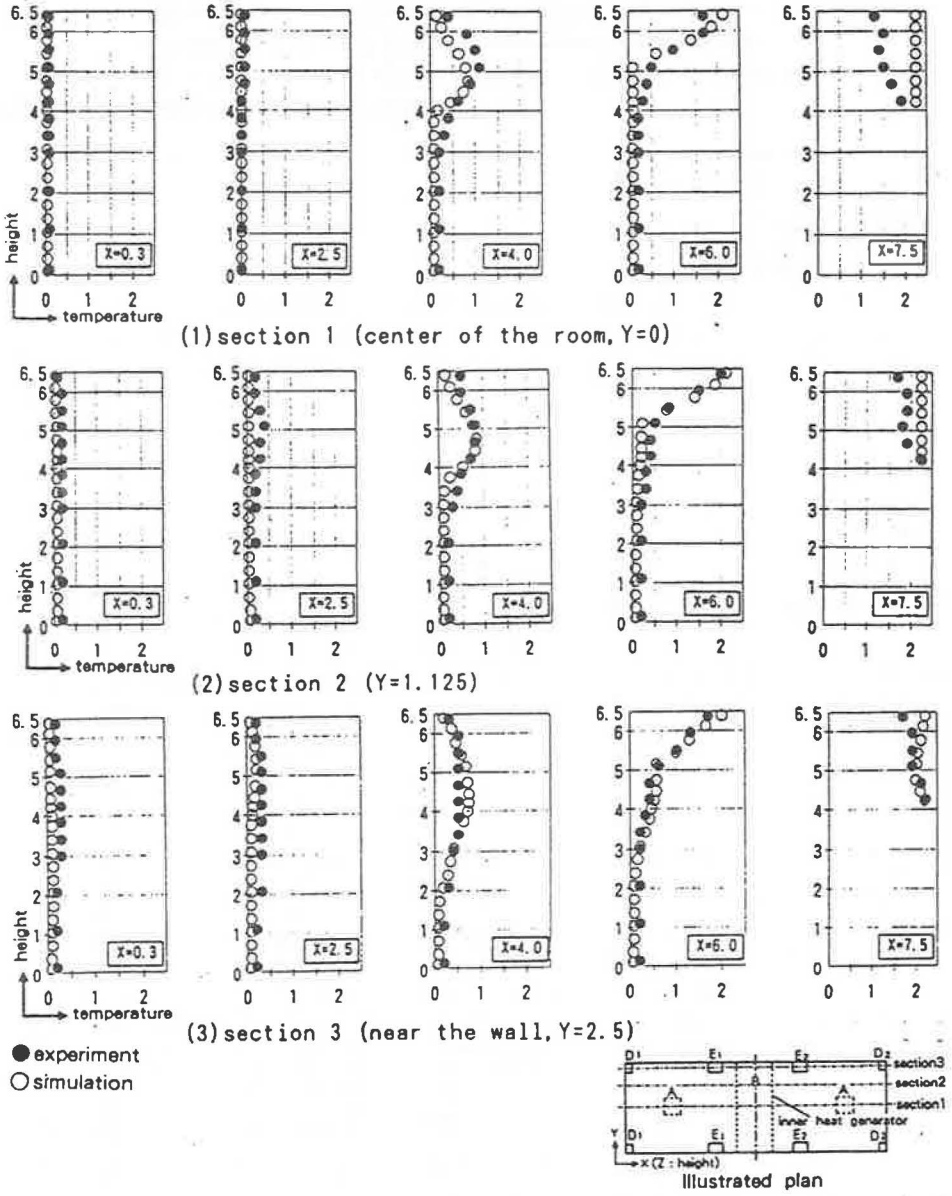

Figure 18 *Temperature distribution in Case 3*
(1) section 1 (center of the room, Y = 0) (a) experiment (b) simulation
(2) section 2 (Y = 1.125) (a) experiment (b) simulation
(3) section 3 (near the wall, Y = 2.5) (a) experiment (b) simulation.

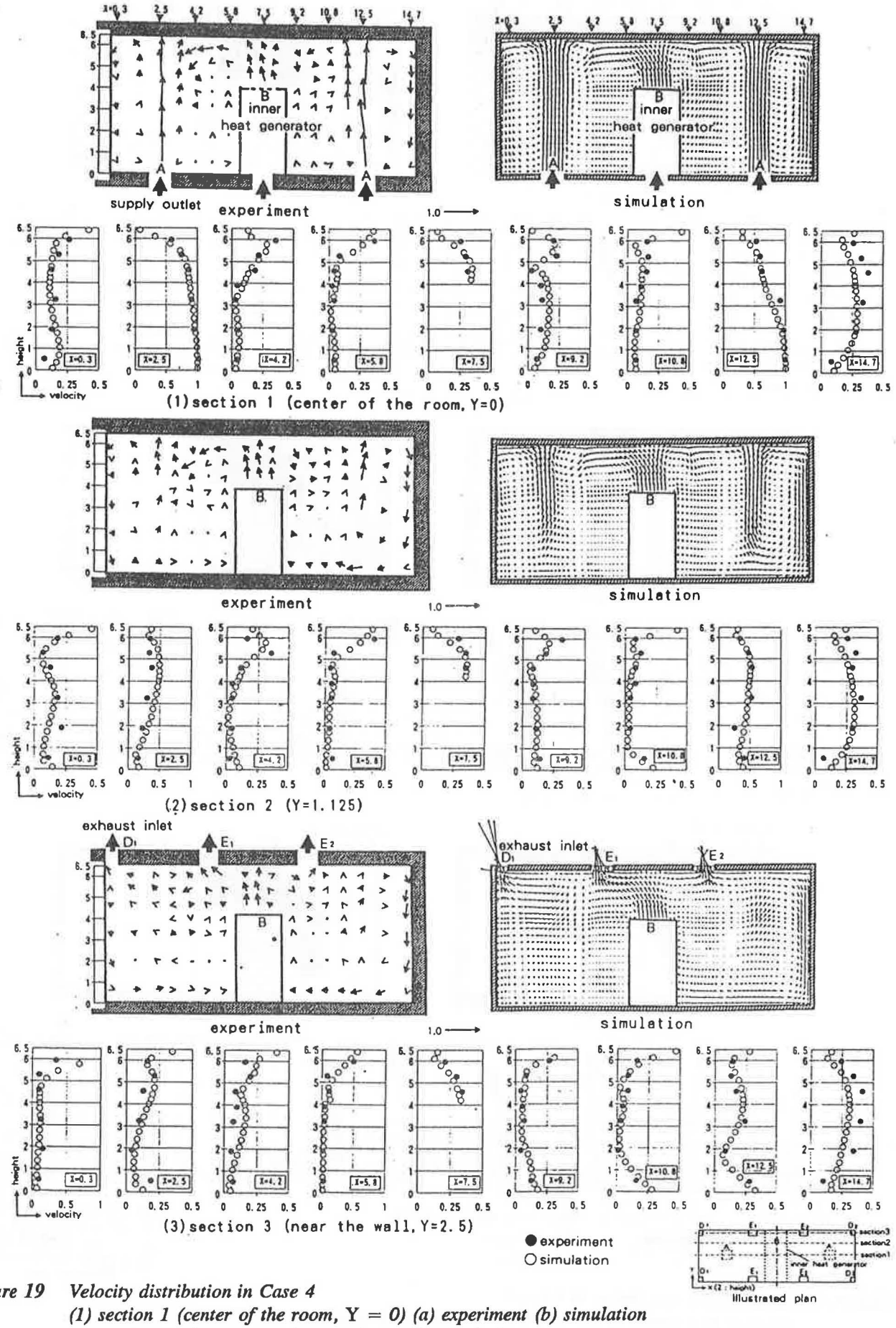

Figure 19 Velocity distribution in Case 4
(1) section 1 (center of the room, Y = 0) (a) experiment (b) simulation
(2) section 2 (Y = 1.125) (a) experiment (b) simulation
(3) section 3 (near the wall, Y = 2.5) (a) experiment (b) simulation.

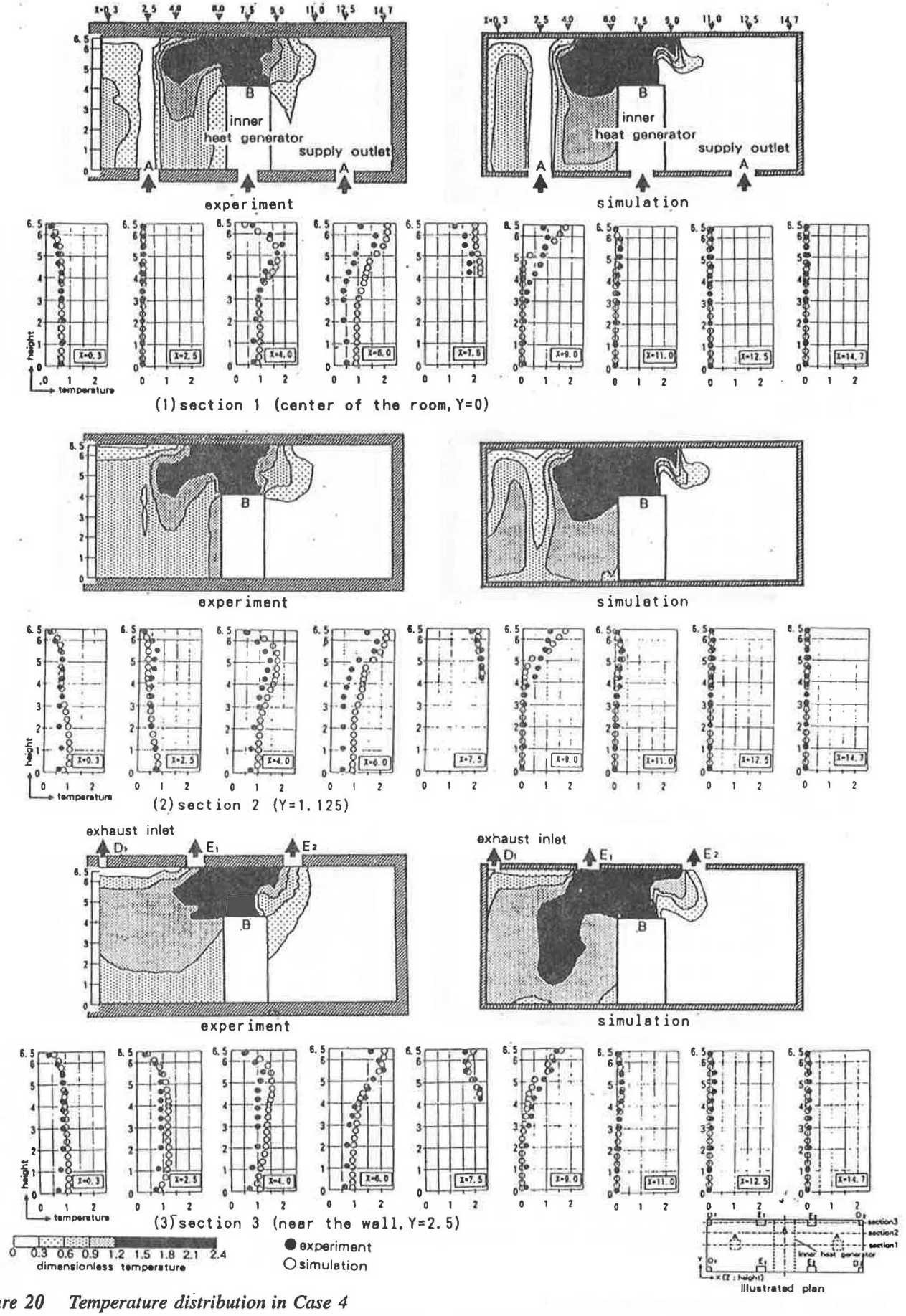

Figure 20 Temperature distribution in Case 4
(1) section 1 (center of the room, Y = 0) (a) experiment (b) simulation
(2) section 2 (Y = 1.125) (a) experiment (b) simulation
(3) section 3 (near the wall, Y = 2.5) (a) experiment (b) simulation.

tion gives a higher temperature than does the experiment.

In Case 4, when the exhausts on the right side of the space are closed, the heat discharged from the model computer diffuses toward the left and does not diffuse toward the right.

CONCLUSIONS

An investigation on flow and temperature distribution in a computer room with a raised floor has been conducted, concentrating especially on the air-exhaust system. A large amount of heat is generated in such rooms by mainframe computers and other equipment. Cooled air is supplied through supply openings in the raised floor, corresponding to the unevenly distributed heat loads. The room air is exhausted through exhaust openings in the ceiling, each of which is designed in accord with the local air supply rate.

Scale-model experiments and numerical simulations based on the k-ε turbulence model were performed to analyze the influence of the exhaust flow rates on the flow and temperature fields.

1. When supply and exhaust airflow rates are locally balanced, most of the heat discharged inside the room can be exhausted near the heat source before it diffuses throughout the whole space.
2. The concept of the flow unit is effective in comprehending a complicated flow and diffusion field with many supply jets.
3. The numerical simulations and the experiments correspond well for the average airflow field, although a few differences can be observed in the jet mixing area and where air flows downward near the wall. However, these differences do not exceed 10% of the supply jet velocity U_o at most measuring points.
4. With regard to temperature distribution, the experiment and the numerical simulation generally correspond well except for the area just above the model computer. However, the difference does not exceed 20% of the representative temperature difference, $\Delta\Theta_o$, at most measuring points.
5. When the supply and exhaust airflow rates are locally imbalanced by decreasing the exhaust airflow rate by 45% in the flow unit where the heat is discharged, the temperature not only of that flow unit but of the whole room becomes higher. This results in less ventilation efficiency when compared with the case where the supply and exhaust airflow rates are locally balanced.
6. When the supply and exhaust airflow rates are locally imbalanced by increasing the exhaust airflow rate by 25% in the flow unit where the heat is generated, the efficiency of heat exhaust is improved in comparison with the case where the supply and exhaust airflow rates are locally balanced.
7. When the exhaust airflow rate between D_1 and D_2 is imbalanced, it causes asymmetries in the flow and diffusion fields. This phenomenon may result in lower ventilation efficiency of the room.

The raised-floor air-conditioning system is an effective method for dealing with unevenly distributed heat loads in a room because supply openings can be precisely allocated in relation to the locations of the heat loads. However, it can become even more effective when the local balance of exhaust and supply airflow is considered.

NOMENCLATURE

Ar	=	Archimedes number = $g\ \beta\ \Delta\ \Theta_o\ L_o/U_o^2$
$C\mu$, $C\varepsilon_1$, $C\varepsilon_2$, $C\varepsilon_3$	=	empirical constants in the k-ε turbulence model
E	=	empirical constant in log law, 9.0 in the case of a smooth wall
G_k	=	production of turbulent kinetic energy by buoyancy
g	=	gravitational acceleration
h	=	length from the wall surface to the center of the adjacent cell
k	=	turbulent kinetic energy
ℓ	=	length scale of turbulence
n_i	=	scale ratio of model to full scale
P_k	=	production of turbulent kinetic energy by mean shear
Re	=	Reynolds number = U_oL_o/ν
Θ	=	temperature
$\Delta\Theta_o$	=	temperature difference between supply and exhaust air
Θ^*	=	dimensionless temperature, $\Theta^* = (\Theta - \Theta_A)/\Delta\Theta_o$
U, V, W	=	X, Y, and Z components of mean velocity vector
U_o	=	representative velocity for nondimensionalization defined by mean velocity at supply outlet
U^*	=	dimensionless velocity, $U^* = U/U_o$
β	=	coefficient of expansion
δ_{ij}	=	Kronecker delta
ε	=	turbulence dissipation rate
κ	=	von Karman constant, 0.4
ν	=	molecular kinematic viscosity
ν_t	=	eddy kinematic viscosity
σ_k, $\sigma\varepsilon$, $\sigma\theta$	=	turbulence Prandtl/Schmidt number of k, ε, and θ (cf. k-ε equation)

REFERENCES

Arnold, D. 1990. Raised floor air distribution—A case study. *ASHRAE Transactions* 96(2): 665-669.

Hanzawa, H., and Y. Nagasawa. 1990. Thermal comfort with underfloor air-conditioning systems. *ASHRAE Transactions* 96(2): 696-698.

Heinemeier, K.E., G.E. Schiller, and C.C. Benton. 1990. Task conditioning for the workplace: Issues and challenges. *ASHRAE Transactions* 96(2): 678-689.

Launder, B.E., and J.L. Spalding. 1974. The numerical computation of turbulent flows. *Computer Method in Applied Mechanics and Engineering* 3: 269-289.

Murakami, S., S. Kato, and Y. Suyama. 1987. Three-dimensional numerical simulation of turbulent airflow in a ventilated room by means of a two-equation model. *ASHRAE Transactions* 93(2): 621-642.

Murakami, S., S. Kato, and Y. Suyama. 1988. Numerical and experimental study on turbulent diffusion fields in conventional-flow-type clean rooms. *ASHRAE Transactions* 94(2): 469-493.

Murakami, S., S. Kato, and Y. Suyama. 1989. Numerical study on diffusion field as affected by arrangement of supply and exhaust openings in conventional-flow-type clean room. *ASHRAE Transactions* 95(2): 113-127.

Murakami, S., S. Kato, and Y. Suyama. 1990a. Numerical study of flow and contaminant diffusion fields as affected by flow obstacles in conventional-flow-type clean room. *ASHRAE Transactions* 96(2): 343-355.

Murakami, S., S. Kato, and Y. Tanaka. 1990b. Study on flow and diffusion field of clean room with locally air-balanced supply-exhaust ventilation system installed at ceiling. *Transactions of SHASEJ* 42: 1-8 (in Japanese).

Murakami, S., S. Kato, and H. Nakagawa. 1991. Numerical prediction of horizontal nonisothermal 3-D jet in room based on the k-ε model. *ASHRAE Transactions* 97(1): 38-48.

Sodec, F., and R.L. Craig. 1990. The underfloor air supply system—The European experience. *ASHRAE Transactions* 96(2): 690-695.

Spoormaker, H.J. 1990. Low-pressure underfloor HVAC system. *ASHRAE Transactions* 96(2): 670-677.

Viollet, P.L. 1987. The modeling of turbulent recirculating flows for the purpose of reactor thermal-hydraulic analysis. *Numerical Engineering and Design* 99: 365-377.